Inorganic Chemistry

Article

pubs.acs.org/IC

One-Electron Oxidation Chemistry and Subsequent Reactivity of Diiron Imido Complexes

Subramaniam Kuppuswamy,[†] Tamara M. Powers,[‡] Bruce M. Johnson,[§] Carl K. Brozek,[∥] Jeremy P. Krogman,[†] Mark W. Bezpalko,[†] Louise A. Berben,[§] Jason M. Keith,[#] Bruce M. Foxman,[†] and Christine M. Thomas*[,†]

[†]Department of Chemistry, Brandeis University, 415 South Street, MS 015, Waltham, Massachusetts 02454, United States

[‡]Department of Chemistry and Chemical Biology, Harvard University, 12 Oxford Street, Cambridge, Massachusetts 02139, United States

[§]Department of Chemistry, University of California, 1 Shields Avenue, Davis, California 95616, United States

[∥]Department of Chemistry, Massachusetts Institute of Technology, 77 Massachusetts Avenue, Cambridge, Massachusetts 02139, United States

[#]Department of Chemistry, Colgate University, 13 Oak Drive, Hamilton, New York 13346, United States

Supporting Information

ABSTRACT: The chemical oxidation and subsequent group transfer activity of the unusual diiron imido complexes Fe(^{i}PrNPPh$_2$)$_3$Fe≡NR (R = *tert*-butyl (^{t}Bu), **1**; adamantyl, **2**) was examined. Bulk chemical oxidation of **1** and **2** with Fc[PF$_6$] (Fc = ferrocene) is accompanied by fluoride ion abstraction from PF$_6^-$ by the iron center *trans* to the Fe≡NR functionality, forming F−Fe(^{i}PrNPPh$_2$)$_3$Fe≡NR (^{i}Pr = isopropyl) (R = ^{t}Bu, **3**; adamantyl, **4**). Axial halide ligation in **3** and **4** significantly disrupts the Fe−Fe interaction in these complexes, as is evident by the >0.3 Å increase in the intermetallic distance in **3** and **4** compared to **1** and **2**. Mössbauer spectroscopy suggests that each of the two pseudotetrahedral iron centers in **3** and **4** is best described as Fe^{III} and that one-electron oxidation has occurred at the tris(amido)-ligated iron center. The absence of electron delocalization across the Fe−Fe≡NR chain in **3** and **4** allows these complexes to readily react with CO and ^{t}BuNC to generate the Fe^{III}Fe^I complexes F−Fe(^{i}PrNPPh$_2$)$_3$Fe(CO)$_2$ (**5**) and F−Fe(^{i}PrNPPh$_2$)$_3$Fe(^{t}BuNC)$_2$ (**6**), respectively. Computational methods are utilized to better understand the electronic structure and reactivity of oxidized complexes **3** and **4**.

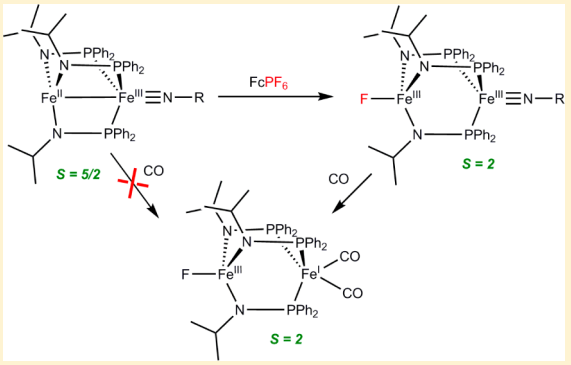

INTRODUCTION

High valent metal imido functionalities have been proposed as intermediates in many chemical transformations such as aziridination, hydrocarbon amination, and nitrene group transfer processes, and iron imidos, in particular, may be relevant to biological nitrogen fixation.[1−9] To date, monometallic iron imido complexes have been isolated and structurally characterized with a wide range of Fe oxidation states from +II to +V,[9−22] but terminal Fe imido fragments in multimetallic assemblies remain less common.[23] Recently, our laboratory reported the first examples of diiron terminal imido complexes, Fe(^{i}PrNPPh$_2$)$_3$Fe≡NR (^{i}Pr = isopropyl) (R = *tert*-butyl (^{t}Bu) (**1**), adamantyl, (**2**), and 2,4,6-trimethylphenyl), in which the imido fragment is situated *trans* to a direct Fe−Fe bond.[24]

A number of reports in recent years have demonstrated enhanced reactivity of the multiply bonded ligands *trans* to metal−metal multiple bonds as the result of delocalized 3-center-4-electron bonding weakening the metal−ligand multiple bond. For example, the diruthenium nitride complex Ru(dPhf)$_4$Ru≡N (dPhf = *N*,*N*′-diphenylformamidinate) and the ditungsten oxo complex [W$_2$O(2,2′-dipyridylamide)$_4$]$^{2+}$ are more active than their monometallic analogues toward C−H amination and oxygen atom transfer, respectively.[25−27] This phenomenon has been exploited most widely in the chemistry of dirhodium complexes such as dirhodium tetraacetate derivatives, which are active catalysts for C−H functionalization reactions proposed to proceed through electrophilic dirhodium carbene and nitrene intermediates.[28] In contrast, however, diiron imido complexes **1** and **2** were shown to be unreactive toward substrates such as CO and organic isocyanide reagents, to which monometallic terminal iron imido complexes are well-known to transfer the nitrene functional group.[13,29] In an effort to better understand the factors that affect the interplay between metal−metal bonds and metal−ligand multiple bonds oriented in a *trans* arrangement, we now turn our attention to

Received: December 10, 2013
Published: May 15, 2014

   dx.doi.org/10.1021/ic403039x | *Inorg. Chem.* 2014, 53, 5429−5437

oxidized variants of **1** and **2** and their reactivity toward oxidative group transfer reactions.

RESULTS AND DISCUSSION

One-Electron Oxidation of 1 and 2. As previously reported, cyclic voltammetry of complexes **1** and **2** revealed reversible oxidative events at −0.32 and −0.35 V (vs Fc/Fc^{+}).[24] Likewise, the chemical oxidation of these two complexes was explored. Stirring complex **1** with $Fc[PF_6]$ in tetrahydrofuran (THF) proceeds smoothly to generate the one-electron oxidized reddish-brown complex **3** in moderate yield. Rather than the ionic Fe^{IV} imido complex $[Fe(\mu\text{-}^{i}PrNPPh_2)_3Fe{\equiv}N^{t}Bu][PF_6]$ that might have been expected based on monometallic analogues,[10,13] complex **3** was identified as $F{-}Fe(\mu\text{-}^{i}PrNPPh_2)_3Fe{\equiv}N^{t}Bu$, the product of fluoride ion abstraction by the one-electron oxidized complex (Scheme 1). Monitoring the reaction by NMR spectroscopy reveals the

Scheme 1

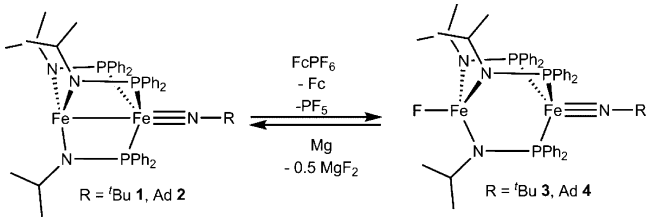

formation of PF_5 as a byproduct by ^{19}F (δ −71.0 ppm, $^{1}J_{F-P}$ = 710 Hz) and ^{31}P NMR (δ −84.0 ppm, $^{1}J_{P-F}$ = 710 Hz) spectroscopy (see Supporting Information). The analogous complex $F{-}Fe(\mu\text{-}^{i}PrNPPh_2)_3Fe{\equiv}NAd$ (**4**) was also formed upon oxidation of complex **2** with $Fc[PF_6]$ under similar reaction conditions. We note that the oxidative feature in the cyclic voltammogram of complex **1** is reversible and does not vary when the supporting electrolyte is changed from $[^{n}Bu_4N][PF_6]$ to $[^{n}Bu_4N][ClO_4]$, suggesting that halide abstraction is a relatively slow process and does not occur on the time scale of electrochemical experiments (Supporting Information, Figure S5). A similar fluoride ion abstraction reaction was observed by Deng and co-workers upon oxidation of the diiron(II) bis(μ-imido) complex $[(NHC)Fe(\mu_2\text{-}NDipp)]_2$ (Dipp = 2,6-diisopropylphenyl, NHC = 2,5-diisopropyl-3,4-dimethylimidazol-1-ylidene) with ferrocenium salts containing $[BF_4]^{-}$ anions.[30] Oxidation of **1** with $Fc[BF_4]$ also leads to halide abstraction and formation of complex **3** (Supporting Information, Figure S3). The ^{1}H NMR spectra of complexes **3** and **4** display five and seven resonances in the δ 15.0 to δ −7.0 range, respectively, indicating C_3-symmetric structures in solution. Cyclic voltammetry of complexes **3** and **4** reveals a reversible reduction at $E_{1/2}$ = −1.3 V, and treatment of **3** and **4** with relatively mild reductants such as Mg or Zn quantitatively regenerates **1** and **2**.

X-ray quality single crystals of **3** and **4** were obtained by slow evaporation of concentrated diethyl ether solutions at room temperature. X-ray crystallography confirms the formulations of these complexes, and the molecular structures of **3** (left) and **4** (right) are depicted in Figure 1. Selected structural parameters of these complexes are given in Table 1. Both iron centers in **3** and **4** adopt a distorted tetrahedral geometry with the fluoride and imido functionalities occupying the apical positions at either end of the molecule. The most notable structural feature of these oxidized complexes is that their Fe−Fe distances (2.9330(3) Å (**3**) and 2.8796(4) Å (**4**)) have increased substantially compared to their precursors **1** and **2** (2.5444(3) Å (**1**) and 2.5443(3) Å (**2**)[24]). The bond metrics associated with the Fe imido fragments of **3** and **4** are otherwise in line with **1** and **2** and with previously reported low-spin tris(phosphine) Fe(III) imide complexes.[11,13,15] For example, the Fe−P distances in **3** ($Fe{-}P_{avg}$ = 2.22 Å) (avg = average) are nearly identical to those in **1** ($Fe{-}P_{avg}$ = 2.23 Å).[24] In contrast, dramatic structural changes are observed at the tris(amido) Fe center in complexes **3** and **4**. As the Fe center moves out of the plane of the three amide nitrogen atoms and its geometry becomes more tetrahedral, the Fe−N distances are significantly elongated ($Fe{-}N_{avg}$ = 1.97 Å) compared to the starting materials **1** and **2** ($Fe{-}N_{avg}$ = 1.94 Å). These structural changes suggest that the tris(amido)Fe center has been oxidized from Fe^{II} to Fe^{III}, leading to halide ion abstraction from PF_6^{-}.

One of the most interesting aspects of complexes **1** and **2** is the presence of two Fe centers in different oxidation and spin states, high-spin Fe^{II} and low-spin Fe^{III}, within the same molecule due to different coordination environments.[24] In complexes **3** and **4**, a similar phenomenon is to be expected with the two Fe centers in the same oxidation state (Fe^{III}) but different spin states. Measurement of the solution magnetic moments of **3** and **4** using the Evans method reveals μ_{eff} values of 4.83 and 4.62 μ_B, respectively, consistent with the S = 2

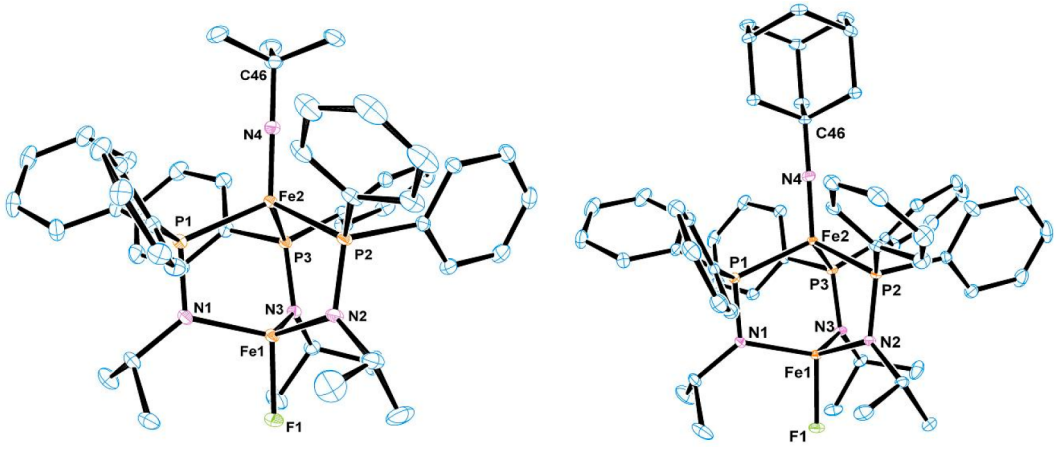

Figure 1. Displacement ellipsoid (50%) representations of **3** (left) and **4** (right). Hydrogen atoms are omitted for clarity.

dx.doi.org/10.1021/ic403039x | Inorg. Chem. 2014, 53, 5429−5437

Table 1. Relevant Interatomic Distances (Å) and Angles (degrees) in Complexes 3−6

	3	4	5	6
Fe1−Fe2	2.9330(3)	2.8796(4)	3.2856(4)	3.2792(8)
Fe1−N1	1.9690(15)	1.9681(14)	1.9587(15)	1.966(3)
Fe1−N2	1.9753(15)	1.9619(13)	1.9533(15)	1.949(3)
Fe1−N3	1.9661(16)	1.9718(14)	1.9563(15)	1.955(3)
Fe1−F1	1.8347(11)	1.8328(10)	1.8188(10)	1.832(2)
Fe2−P1	2.2290(5)	2.2255(5)	2.3189(5)	2.2877(11)
Fe2−P2	2.2205(5)	2.2238(5)	2.3128(5)	2.2739(11)
Fe2−P3	2.2149(5)	2.2206(5)	2.2394(5)	2.2764(11)
Fe2−N4	1.6251(15)	1.6268(15)		
N1−Fe1−N2	114.46(7)	116.89(6)	115.43(6)	109.05(12)
N1−Fe1−N3	114.49(6)	116.69(6)	108.19(6)	113.47(12)
N2−Fe1−N3	115.47(7)	112.59(6)	112.96(6)	114.17(12)

ground states that are expected upon removal of an electron from the $S = 5/2$ precursors **1** and **2**. An $S = 2$ ground state might be expected to result from antiferromagnetic coupling of the single electron on the low-spin Fe^{III} center with one of the five unpaired electrons on a high-spin Fe^{III} center. Solid-state magnetic susceptibility measurements determined using superconducting quantum interference device (SQUID) magnetometry for **3** support this assignment (Figure 2). At 300 K the

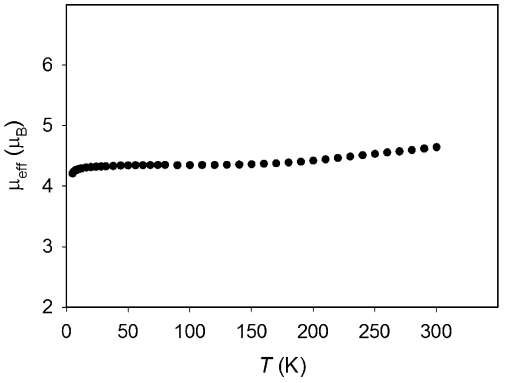

Figure 2. Variable-temperature magnetic susceptibility data for compound **3** in the solid state in an applied field of 0.1 T determined using SQUID magnetometry.

observed magnetic moment is 4.64 μ_B, which is in good agreement with both the solution measurement and the predicted magnetic moment of 4.83 μ_B for the $S = 2$ system (assuming $g = 2.0$). The drop in the measured magnetic moment to 4.21 μ_B at 5 K could be attributed to several possibilities, such as intermolecular antiferromagnetic interactions, zero-field splitting, or a very slow spin crossover process. The proposal that the iron centers are interacting antiferromagnetically is also in agreement with the predictions made using density functional theory (DFT) calculations (*vide infra*).

To further probe the electronic structure of complexes **3** and **4**, a zero-field ^{57}Fe Mössbauer spectrum of complex **3** was collected (Figure 3). The Mössbauer spectrum features two quadrupole doublets centered at $\delta = 0.26$ mm/s ($|\Delta E_Q| = 1.28$ mm/s) and $\delta = -0.12$ mm/s ($|\Delta E_Q| = 2.70$ mm/s), further confirming the disparity between the two different iron centers in this complex. A third signal of lesser intensity (10%, $\delta = 0.52$ mm/s ($|\Delta E_Q| = 2.40$ mm/s)) is also observed as the result of a residual ferrocene impurity.[31] The isomer shift centered at $\delta = -0.12$ mm/s is assigned to the imido-bound low-spin Fe^{III}

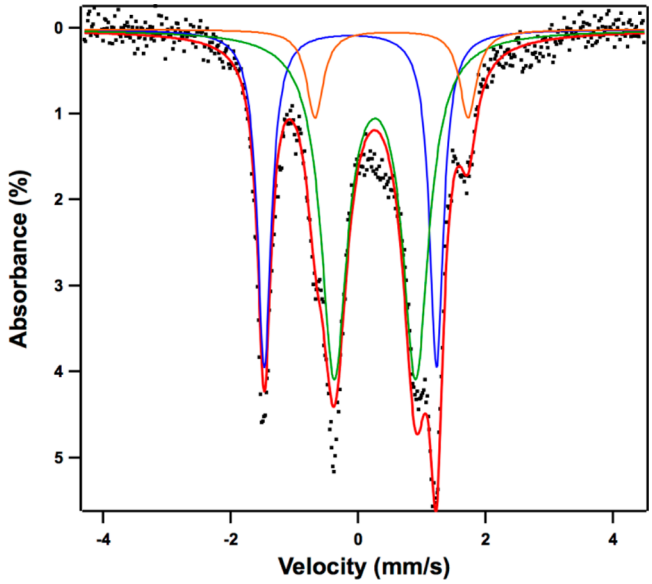

Figure 3. ^{57}Fe Mössbauer spectrum of a solid sample of **3** at 90 K (black dotted lines). The spectrum was adequately fit (red) as a combination of two signals ($\delta = 0.26$ mm/s, $|\Delta E_Q| = 1.28$ mm/s, $\Gamma = 0.13$ mm/s, (58%, green); $\delta = -0.12$ mm/s, $|\Delta E_Q| = 2.70$ mm/s, $\Gamma = 0.25$ mm/s (32%, blue)), along with a ferrocene impurity ($\delta = 0.52$ mm/s, $|\Delta E_Q| = 2.40$ mm/s, $\Gamma = 0.16$ mm/s (10%, orange)).

center based on comparison to the isomer shift of the imido−Fe^{III} center in the precursor complex **1** ($\delta = -0.06$ mm/s).[24] This value is also consistent with the Mössbauer isomer shift reported for the low-spin Fe^{III} complex PhB(MesIm)$_3$Fe≡NAd ($\delta = -0.11$ mm/s)[32] and is higher than the isomer shifts reported for low-spin C_3-symmetric Fe^{IV} complexes (e.g., PhB(MesIm)$_3$Fe≡N, $\delta = -0.28$ mm/s;[32] PhB(^{t}BuIm)$_3$Fe≡N, $\delta = -0.28$ mm/s;[32,33] PhB(CH$_2$P^{i}Pr$_2$)$_3$Fe≡N, $\delta = -0.34$ mm/s;[34] (TIMEN^{Mes})Fe≡N, $\delta = -0.27$ mm/s[35]). Notably, the quadrupole splitting observed for this signal is significantly larger than that observed for **1** (0.54 mm/s), a phenomenon that may be attributed to the absence of metal−metal bonding in **3**. The isomer shift at $\delta = 0.26$ mm/s, attributed to the tris(amido)Fe center, is considerably lower than that for the tris(amido)Fe^{II} centers in the similarly ligated complexes [Fe(^{i}PrNPPh$_2$)$_3$Fe(^{i}PrNPPh$_2$)] ($\delta = 0.56$ mm/s)[36] and [Fe(^{i}PrNPPh$_2$)$_3$Cu$_2$(^{i}PrNPPh$_2$)] ($\delta = 0.65$ mm/s),[37] consistent with oxidation from Fe^{II} to Fe^{III}.

To corroborate our assignment of each quadrupole doublet in the Mössbauer spectrum of **3** to the two respective Fe

dx.doi.org/10.1021/ic403039x | Inorg. Chem. 2014, 53, 5429−5437

centers, computational methods were used to predict the isomer shift and quadrupole splitting of each Fe center. The calculated Mössbauer parameters are in good agreement with our intuitive assignment: the imido-bound Fe center is predicted to have an isomer shift of δ = −0.28 mm/s and a $|\Delta E_Q|$ = 2.57 mm/s, while the computed parameters for the tris(amido) Fe center are δ = 0.18 mm/s and $|\Delta E_Q|$ = 1.48 mm/s.

Reactivity of 3 and 4 toward Nitrene Transfer. Complexes **1** and **2** were previously reported to be unreactive toward nitrene transfer to carbon monoxide or isocyanide reagents,[24] in contrast to monometallic Fe(III) imido analogues.[13] This difference was attributed to both steric (diminished accessibility to the Fe≡NR fragment) and electronic factors (stabilization of Fe−N π symmetry orbitals), each of which results from the wider P−Fe−P angles that occur as a result of the Fe−Fe interaction. As the Fe−Fe interaction is disrupted upon one-electron oxidation and fluoride ion abstraction, complexes **3** and **4** might be expected to show enhanced reactivity toward nitrene transfer. Indeed, complex **3** quantitatively reacts with CO (1 atm) at room temperature to generate two-electron reduced F−Fe(^{i}PrNPPh$_2$)$_3$Fe(CO)$_2$ (**5**) as a red microcrystalline solid in 80% isolated yield, with concomitant elimination of ^{t}BuNCO (Scheme 2). Complex **3** is also reactive toward isocyanide reagents: treatment of complex **3** with 3 equiv of ^{t}BuNC at room temperature gives rise to Fe(^{i}PrNPPh$_2$)$_3$Fe(CN^{t}Bu)$_2$ (**6**) in 75% isolated yield, eliminating ^{t}BuN=C=N^{t}Bu. The isocyanate and carbodiimide byproducts extruded during the reactions to form **5** and **6** were identified by GC/MS and by characteristic IR stretches at 2280 and 2271 cm^{-1}. The four broad paramagnetically shifted resonances observed in the ^{1}H NMR spectrum of **5** between δ 16.0 and 1.7 ppm suggest a relatively symmetric geometry in solution. A similar ^{1}H NMR spectrum is observed for complex **6** with an additional resonance observed at 0.8 ppm assigned to the ^{t}Bu groups on the ^{t}BuN≡C ligands. In contrast to monometallic systems, addition of ^{t}BuN$_3$ to complex **5** does not regenerate imido complex **3**, precluding catalytic nitrene transfer.[29]

Scheme 2

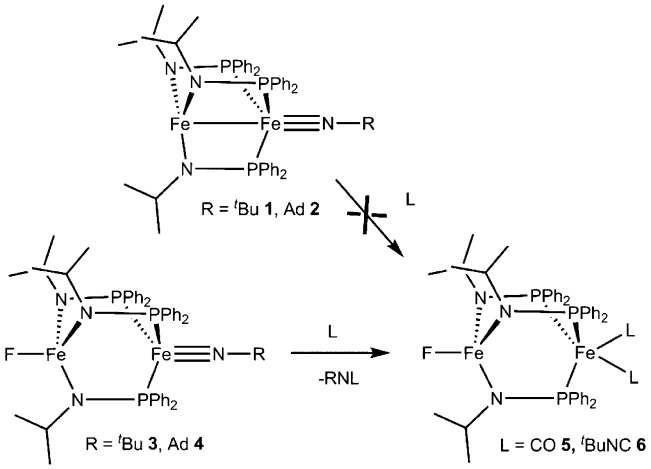

The chemical formulations of **5** and **6** were further confirmed by X-ray crystallography; their solid-state structures are shown in Figure 4, and their bond metrics are tabulated in Table 1. The tris(phosphine)Fe(L)$_2$ fragment in both complexes adopts a distorted square pyramidal geometry (τ = 0.03 for **5** and 0.02 for **6**),[38] suggesting that the equivalence of the phosphinoamide ligands by ^{1}H NMR spectroscopy is the result of fluxionality in solution. The Fe−Fe interatomic distance in **5** and **6** is considerably longer than that in **3** and **4** (3.2856(4) Å (**5**) and 3.2792(8) Å (**6**) vs 2.9330(3) Å (**3**) and 2.8796(4) Å (**4**)), but since there is no metal−metal interaction in either pair of complexes, this can be attributed to the Fe center moving further out of the plane of the three phosphorus atoms to accommodate a fifth ligand. Consistent with reduction of the tris(phosphine)Fe center, the Fe−P distances are elongated in Fe^{III}Fe^{I} **5** and **6** with respect to Fe^{III}Fe^{III} precursors **3** and **4** (Table 1). The geometry at the tris(amido)Fe center remains pseudotetrahedral, with geometric parameters largely similar to those of **3** and **4**.

Complexes **5** and **6** present another unusual scenario where each metal in the bimetallic complex is expected to adopt a different spin state. While the tris(amido)Fe^{III}−F center remains high-spin and in a weak ligand field, the strong-field CO ligands on the tris(phosphine)Fe^{I} fragment promote a low-spin configuration. Interestingly, the solution magnetic moments of **5** and **6** are 4.86 and 4.89 μ_B, indicative of the S = 2 electronic configuration similar to that observed for complexes **3** and **4**. Antiferromagnetic coupling of the single unpaired

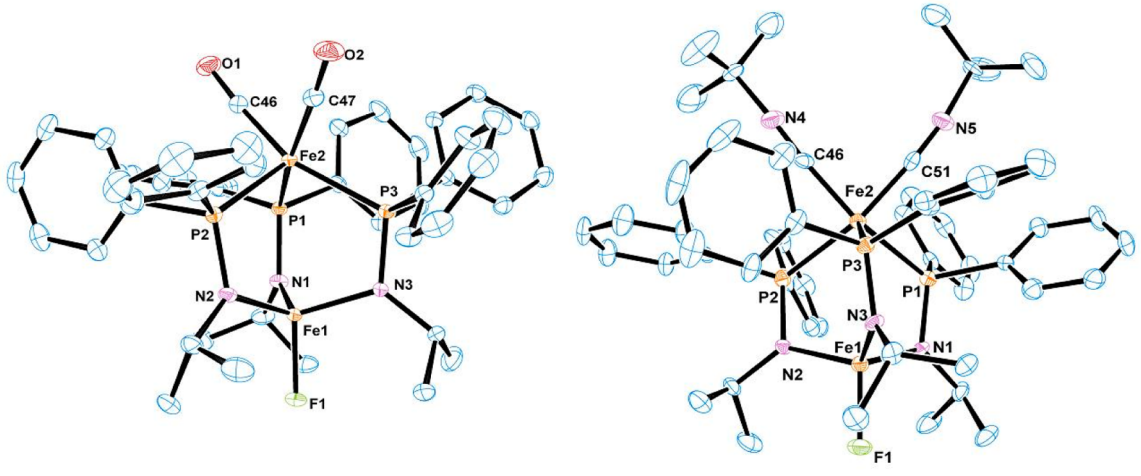

Figure 4. Displacement ellipsoid (40%) representations of **5** (left) and **6** (right). Hydrogen atoms are omitted for clarity.

dx.doi.org/10.1021/ic403039x | Inorg. Chem. 2014, 53, 5429−5437

electron on the low-spin $Fe^{I}(CO)_2$ fragment with one of the five unpaired electrons on the high-spin tris(amido)Fe^{III}–F fragment, would again account for the observed $S = 2$ ground states of **5** and **6**. The variable-temperature magnetic susceptibility of complex **5** was further investigated using SQUID magnetometry; the observed magnetic moment at 300 K is 4.93 μ_B, and this is consistent with both the solution measurement and an electronic structure that has four unpaired electrons (Figure 5). As in complex **3**, the measured magnetic

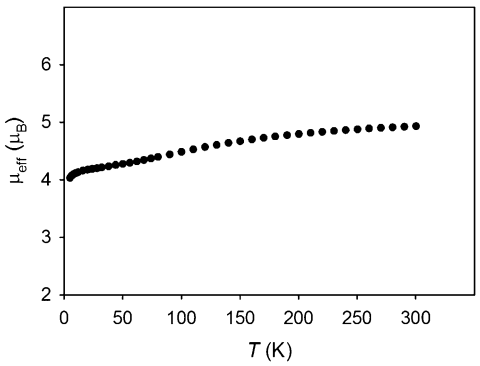

Figure 5. Variable-temperature magnetic susceptibility data for compound **5** in the solid state in an applied field of 0.1 T determined using SQUID magnetometry.

moment of **5** falls slightly at 5 K, in this case to 4.03 μ_B. Once again this behavior suggests the presence of weak intermolecular antiferromagnetic coupling or possibly a zero-field splitting effect.

To further probe the reduced oxidation state assignment of complexes **5** and **6**, complex **5** was examined by ^{57}Fe Mössbauer spectroscopy. As shown in Figure 6, the Mössbauer spectrum of **5** shows two quadrupole doublets centered at δ = 0.20 mm/s ($|\Delta E_Q|$ = 1.24 mm/s) and 0.08 mm/s ($|\Delta E_Q|$ = 0.37

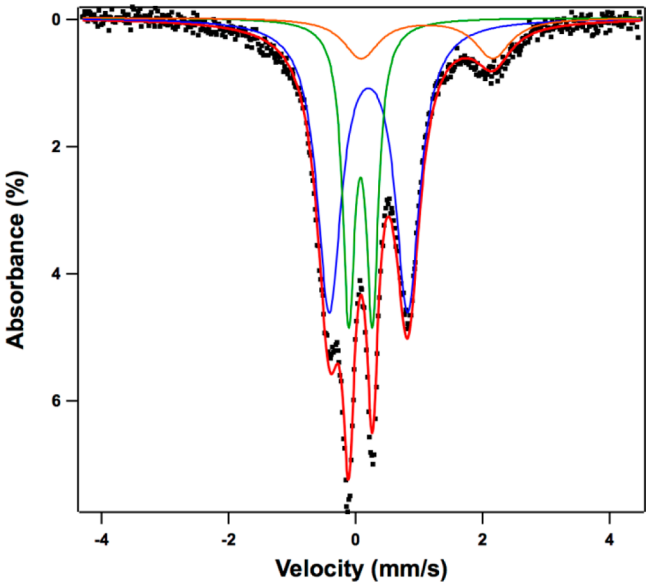

Figure 6. ^{57}Fe Mössbauer spectrum of a solid sample of **5** at 90 K (black dotted lines) fitted (red) as two signals δ = 0.20 mm/s; $|\Delta E_Q|$ = 1.24 mm/s, Γ = 0.23 mm/s (58%, blue) and δ = 0.08 mm/s; $|\Delta E_Q|$ = 0.37 mm/s, Γ = 0.12 mm/s (30%, green) along with an impurity at δ = 1.1 mm/s; $|\Delta E_Q|$ = 2.07 mm/s, Γ = 0.34 mm/s (12%, orange).

mm/s). On the basis of the similarity of both the isomer shift and quadrupole splitting of the signal at 0.20 mm/s to that observed in **3**, this doublet is assigned to the tris(amido)Fe center, which remains in a high-spin Fe^{III} state. The doublet centered at 0.08 mm/s is, therefore, attributed to the Fe center in the tris(phosphine)$Fe(CO)_2$ fragment. There are few low-spin Fe^{I} complexes with Mössbauer parameters available for comparison; however, we note that the 0.08 mm/s isomer shift is relatively low compared to other low-spin Fe^{I} carbonyl complexes reported in the literature, including Riordan's $PhB(CH_2S^tBu)_3Fe(CO)_2$ complex (δ = 0.21 mm/s, $|\Delta E_Q|$ = 0.47 mm/s)[39] and Chirik's $[(^i PrPDI)Fe(CO)_2]^+$ complex (δ = 0.17 mm/s, $|\Delta E_Q|$ = 0.62 mm/s).[40] Again, we turned to computational methods to validate our assignment of each set of Mössbauer parameters to the two Fe centers. The calculated Mössbauer parameters are consistent with our assignment. The $Fe(CO)_2$ center in **5** is predicted to have an isomer shift of δ = −0.08 mm/s and a $|\Delta E_Q|$ = 0.46 mm/s, while the computed parameters for the tris(amido) Fe center are δ = 0.21 mm/s and a $|\Delta E_Q|$ = 1.37 mm/s.

The best evidence for the low-spin Fe^{I} oxidation state assignment of the tris(phosphine)-ligated $Fe(CO)_2$ fragment is the IR carbonyl stretching frequencies. The IR spectrum of complex **5** exhibits two diagnostic ν_{CO} stretches at 1982 and 1921 cm^{-1}, which are consistent with those reported for the similarly ligated $Fe^{I}(CO)_2$ fragment in $PhB(CH_2PPh_2)_3Fe(CO)_2$ (ν_{CO} = 1979 and 1914 cm^{-1})[13] or the tris(thioether) complex $PhB(CH_2S^tBu)_3Fe(CO)_2$ ((ν_{CO} = 1984 and 1911 cm^{-1}).[39] The ultraviolet–visible–near-infrared (UV–vis–NIR) spectrum of mixed-valence complex **5** also has a low-intensity broad absorption at 878 nm that is not present in complex **3**. This feature may be assigned to intervalence charge transfer (Supporting Information, Figure S12).

Computational Studies. To better understand the electronic structure of the oxidized imido complexes **3** and **4**, a computational investigation was undertaken using DFT. We first investigated the oxidized $S = 2$ diiron imido cation $[Fe(^i PrNPPh_2)_3Fe{\equiv}N^tBu]^+$ (**7**) that would be formed upon oxidation of **3** prior to halide abstraction. The molecular orbital diagram of **7** is largely similar to that reported for **3**,[24] with an electron removed from the highest-energy singly occupied molecular orbital (SOMO): the metal–metal σ^* orbital (Figure 7 and Supporting Information). Consequently, the DFT-optimized geometry of **7** reveals a shorter Fe–Fe distance (2.41 Å in **7** compared to 2.5443(3) Å in **3**).[24] The lowest unoccupied molecular orbital (LUMO) of this electrophilic cation (shown in Figure 7) is Fe–Fe σ^* in character, with repulsion of the Fe d_{z^2} orbitals polarizing the empty d_{z^2} lobe of the tris(amido)Fe center in the direction of the open coordination site and promoting F^- abstraction.

Upon fluoride ion abstraction to generate complex **3**, the geometry at the tris(amido)Fe center changes to pseudotetrahedral, leading to a weaker ligand field as the $d_{x^2-y^2}$- and d_{xy}-derived orbitals lower in energy, while the d_{xz} and d_{yz} orbitals are destabilized. This is evident in the overall molecular orbital picture of **3** (Figure 7), but the most important change resulting from fluoride ion abstraction is the destabilization of the d_{z^2} orbital of the fluoride-bound Fe center as it becomes antibonding with respect to F^-. This serves to substantially weaken the Fe–Fe interaction in **3**, likely in combination with geometric constraints that impose an elongated intermetallic distance between the two tetrahedral Fe centers.

dx.doi.org/10.1021/ic403039x | Inorg. Chem. 2014, 53, 5429–5437

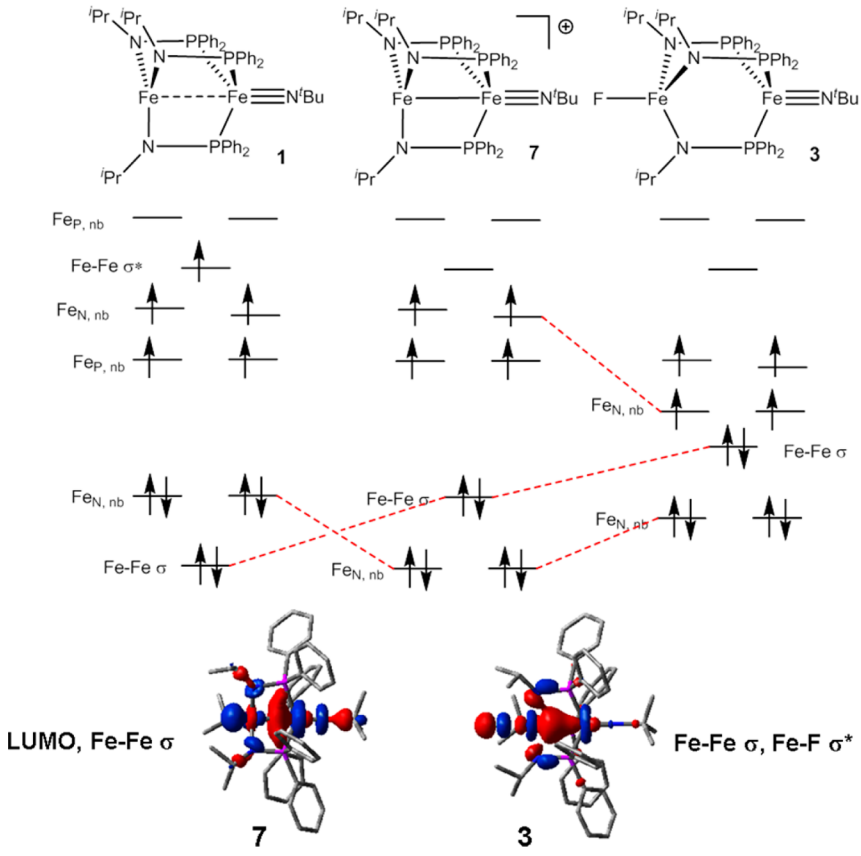

Figure 7. Qualitative frontier molecular orbital diagrams of precursor **1**, oxidized intermediate **7**, and fluoride abstraction product **3** predicted computationally. Representative pictorial representations of the LUMO of complex **7** and the Fe−Fe σ bonding orbital of **3** are shown.

To explore the magnetic interaction between the two Fe centers in complex **3** as well as in the dicarbonyl complex **5**, additional computational studies were carried out. In both cases, the antiferromagnetically coupled quintet state was lower in energy than the ferromagnetically coupled septet state, and the optimized Fe−Fe distance for the $S = 2$ state matched best with the X-ray derived experimental Fe−Fe interatomic distance. The computed spin densities shown in Figure 8 and

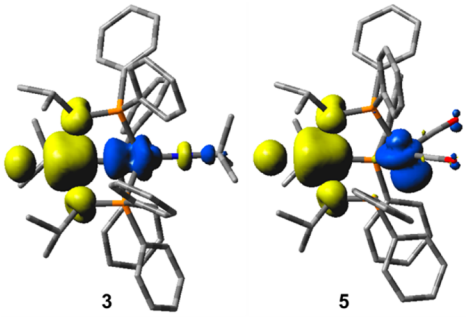

Figure 8. Computed spin density surfaces for the antiferromagnetically coupled $S = 2$ complexes **3** and **5** with α-spin density in yellow and β-spin density in blue.

tabulated in Table 2 reveal a single unpaired electron on the tris(phosphine)Fe center antiferromagnetically coupled to ~5 unpaired electrons distributed throughout the tris(amido) Fe center and the ligand atoms bound to it, consistent with the experimental $S = 2$ ground state.

CONCLUSION

In summary, we have shown that the diiron imido complexes **1** and **2** can be readily oxidized, but the oxidized products are unstable and undergo fluoride ion abstraction from PF_6^- to form the neutral $Fe^{III}Fe^{III}$ imido complexes **3** and **4**. The metal−metal interaction in complexes **3** and **4** is disrupted significantly, and this appears to facilitate reactivity toward nitrene transfer. Indeed, complexes **3** and **4** readily undergo nitrene transfer to CO and ^{t}BuNC at room temperature similar to monometallic Fe^{III} imido complexes,[13,29] while their $Fe^{II}Fe^{III}$ precursors **1** and **2** are unreactive toward these substrates even at elevated temperature. The enhanced reactivity of Fe^{III} imido complexes upon removal of the Fe−Fe interaction is perhaps surprising in light of other bimetallic systems in which metal−metal interactions serve to promote reactivity.[28] However, in contrast to the previously studied examples of M−M=E delocalized systems that show enhanced electrophilicity, the reactivity examined here hinges on the *nucleophilicity* of the imido fragment. The delocalization of electron density through the metal−metal interaction in complexes **1** and **2** serves to attenuate the nucleophilicity of the imido fragment, preventing reactivity with CO or ^{t}BuNC. Upon elimination of the metal−metal interaction in complexes **3** and **4**, however, the Fe≡NR fragment becomes more nucleophilic and reactive toward nitrene transfer for CO and ^{t}BuNC.

EXPERIMENTAL SECTION

General Considerations. Unless specified otherwise, all manipulations were performed under an inert atmosphere using standard Schlenk or glovebox techniques. Glassware was oven-dried before use.

dx.doi.org/10.1021/ic403039x | *Inorg. Chem.* 2014, 53, 5429−5437

Table 2. Computed Mulliken Spin Densities for Selected Atoms in Complexes 3 and 5 in Both the Antiferromagnetically Coupled $S = 2$ State and the Ferromagnetically Coupled $S = 3$ State

	3		5	
	$S = 2$ (Fe−Fe = 2.81 Å)	$S = 3$ (Fe−Fe = 3.32 Å)	$S = 2$ (Fe−Fe = 3.38 Å)	$S = 3$ (Fe−Fe = 3.42 Å)
$Fe_{(PR2)3}$	−0.67	1.18	−0.98	0.97
$Fe_{(NR)3}$	3.81	4.02	4.05	4.07
F	0.18	0.19	0.20	0.21
N	0.16	0.18	0.15	0.18
N	0.16	0.18	0.17	0.20
N	0.16	0.19	0.19	0.17

Benzene, pentane, diethyl ether (Et_2O), THF, and toluene were dried using a Glass Contours solvent purification system. All solvents were stored over 3 Å molecular sieves prior to use. Benzene-d_6 (Cambridge Isotopes) was degassed via repeated freeze−pump−thaw cycles and dried over 3 Å molecular sieves. Complexes [Fe(^{i}PrNPPh$_2$)$_3$Fe≡N^{t}Bu] (**1**) and [Fe(^{i}PrNPPh$_2$)$_3$Fe≡NAd] (**2**) were synthesized using literature procedures.[24] NMR spectra were recorded at ambient temperature on a Varian Inova 400 MHz instrument. Chemical shifts are reported in δ (ppm). For ^{1}H and ^{13}C{^{1}H} NMR spectra, the solvent resonance was used as an internal reference, and for ^{31}P{^{1}H} NMR spectra, 85% H_3PO_4 was referenced as an external standard (0 ppm). ^{19}F NMR spectra were reported with respect to external CF_3CO_2H (−76.5 ppm). IR spectra were recorded on a Varian 640-IR spectrometer controlled by Resolutions Pro software. UV−vis spectra were recorded on a Cary 50 UV−vis spectrophotometer using Cary WinUV software. Gas chromatography−mass spectrometry (GC-MS) data were collected on Agilent 7890A GC System and 5975C VL MSD with Triple-Axis Detector, and yields were reported via integration versus an internal standard (tetradecane). Elemental analyses were performed at Complete Analysis Laboratory Inc., Parsippany, NJ. Solution magnetic moments were measured using the Evans method.[41,42]

Electrochemistry. Cyclic voltammetry measurements were carried out in a glovebox under a dinitrogen atmosphere in a one-compartment cell using a CH Instruments electrochemical analyzer. A glassy carbon electrode and platinum wire were used as the working and auxiliary electrodes, respectively. The reference electrode was Ag/$AgNO_3$ in THF. Solutions of electrolyte (0.40 M [^{n}Bu$_4$N][PF_6] in THF) and analyte (2 mM) were also prepared in the glovebox. All potentials are reported versus an internal ferrocene/ferrocenium reference.

Mössbauer Spectroscopy. ^{57}Fe Mössbauer spectra were measured on a constant acceleration spectrometer (SEE Co, Minneapolis, MN) with a Janis SVT-100 cryostat. Isomer shifts are quoted relative to α-Fe foil (<25 μm thick) at room temperature. The Fe foil standard spectrum has line widths Γ (full width at half-maximum) of 0.292 and 0.326 mm/s for the doublets within the ±4 mm/s window when measured outside the cryostat at room temperature. Samples of **3** and **5** were prepared using approximately 60 mg of sample suspended in paratone-N oil. Data were analyzed using a package written by E. R. King and modified by E. V. Eames in Igor Pro (Wavemetrics) using a simple model consisting of Lorentzian lineshapes with optional asymmetry. Percent components of the quadrupole doublets in the Mössbauer spectra were determined by integrating the individual components' fits and using the areas of those fits to determine the relative area ratios of the quadrupole doublets.

Magnetic Susceptibility Measurements. Solid-state magnetic measurements were recorded using a Quantum Designs MPMS XL magnetometer at 0.1 T. The sample was contained under nitrogen in a gelcap and suspended in the magnetometer in a plastic straw. The magnetic susceptibility was adjusted for diamagnetic contributions using Pascal's constants.

X-ray Crystallography Procedures. All operations were performed on a Bruker-Nonius Kappa Apex2 diffractometer using graphite-monochromated Mo Kα radiation. All diffractometer manipulations, including data collection, integration, scaling, and absorption corrections, were carried out using the Bruker Apex2 software.[43] Preliminary cell constants were obtained from three sets of 12 frames. Data collection and refinement details are presented in Table S1, and fully labeled diagrams and data collection and refinement details are included in the Supporting Information file.

Computational Details. All calculations were performed using Gaussian09-E.01[44] for the Linux operating system. DFT calculations were carried out using a combination of Becke's 1988 gradient-corrected exchange functional[45] and Perdew's 1986 electron-correlation functional[46] (BP86). For open-shell systems, unrestricted wavefunctions were used in energy calculations. A mixed-basis set was employed, using the LANL2TZ(f) triple-ζ basis set with effective core potentials for iron,[47−49] Gaussian09's internal 6-311+G(d) for atoms bonded directly to the metal centers (nitrogen and phosphorus), and Gaussian09's internal LANL2DZ basis set (equivalent to D95V[50]) for carbon and hydrogen. Starting with crystallographically determined geometries as a starting point, when available, the geometries were optimized to a minimum, followed by analytical frequency calculations to confirm that no imaginary frequencies were present.

The unrestricted antiferromagnetically coupled ground state solutions were located through a two-step process: (1) High-spin ($S = 3$) ferromagnetically coupled optimizations were performed; (2) the ferromagnetically coupled solution was used as an initial guess for the intermediate-spin ($S = 2$) antiferromagnetically coupled system. Mulliken spin densities and spin density plots were used to verify that the correct antiferromagnetically coupled state was obtained.

The ORCA 2.9.1[51] computational package was used to optimize the geometry and simulate Mössbauer parameters of a model of compounds **3** and **5**. We employed the pure-DFT functional BP86[45,46] and the Ahlrichs TZV basis sets[52] and polarization functions for all calculations. The self-consistent field equations were converged tightly to 10^{-8} Hartree in the total energy, and the open-shell systems were treated with spin-unrestricted Kohn−Sham determinants. The Broken Symmetry feature was used to specify one unpaired electron on the imido-bound iron site, while four unpaired electrons were imposed on the second site.

We constructed the model compound by starting from the crystal structure and simplifying all −R to methyl groups. The entire structure was optimized with a tolerance of 5×10^{-6} Hartree for each energy change. The electron paramagnetic resonance/NMR module was used to simulate the Mössbauer parameters. Both the spin−spin and spin−orbit operators were evaluated, using the coupled-perturbed method to solve the spin−orbit component. This calculation provided values of η, the asymmetry parameter, and ρ, the s-orbital electron density at the absorbing nucleus. The quadrupole splittings of both iron nuclei were calculated from the values of η. To correlate the computed ρ to an isomer shift value, we calculated ρ for a series of compounds with known isomer shifts and, using their linear relation, determined isomer shifts from a best-fit line. The known compounds were simple iron salts covering a range of oxidation states and were treated in a manner identical to **3** and **5** by starting from reported crystal structures.

*F−Fe(^{i}PrNPPh$_2$)$_3$Fe≡N^{t}Bu (**3**).* A solution of ferrocenium hexafluorophosphate (0.13 g, 0.39 mmol) in THF (3 mL) was chilled to −32 °C, and to this a THF solution of **1** (0.35 g, 0.39 mmol) was added dropwise over a period of 10 min. The reaction mixture slowly turned from reddish-brown to brown and was continuously stirred for

dx.doi.org/10.1021/ic403039x | Inorg. Chem. 2014, 53, 5429−5437

2 h to ensure completion of the reaction to form **3**. Volatiles were removed under vacuum. Extraction of the remaining brown material into Et_2O, followed by removal of volatiles in vacuo yielded analytically pure **3** (0.25 g, 69%). X-ray quality single crystals of **3** were grown upon slow evaporation of a concentrated Et_2O solution of **3** at room temperature. ^1H NMR (400 MHz, C_6D_6): δ 14.7 (18H, ^{i}Pr−CH_3), 7.2 (6H, Ph), 5.5 (9H, N^{t}Bu), 1.3 (12H, Ph), −7.1 (12H, Ph) (isopropyl methine resonance is not observed). UV−vis−NIR (C_6H_6) λ_{max}, nm (ε, L mol^{-1} cm^{-1}): 495 (1600), 667 (400). Evans' method (C_6D_6): 4.83 μ_B. Anal. Calcd for $C_{49}H_{60}FFe_2N_4P_3$: C, 63.38; H, 6.51; N, 6.03. Found: C, 63.46; H, 6.59; N, 5.98%.

F−Fe(^{i}PrNPPh$_2$)$_3$Fe≡NAd (**4**). A solution of ferrocenium hexafluorophosphate (0.075 g, 0.23 mmol) in THF (3 mL) was chilled to −32 °C, and to this a THF solution of **2** (0.23 g, 0.23 mmol) was added dropwise over a period of 10 min. The reaction mixture slowly turned from reddish-brown to brown and was continuously stirred for 2 h to ensure completion of the reaction. Volatiles were removed in vacuo, and the brown crude materials were washed with cold pentane to remove ferrocene and the soluble impurities. Extraction of the remaining brown material into Et_2O, followed by removal of volatiles in vacuo yielded analytically pure **4** (0.17 g, 74%). X-ray quality single crystals of **4** were grown upon slow evaporation of a concentrated Et_2O solution of **4** at room temperature. ^1H NMR (400 MHz, C_6D_6): δ 14.9 (18H, ^{i}Pr−CH_3), 9.4 (6H, Ad), 7.8 (6H, Ph), 4.6 (3H, Ad), 1.3 (12H, Ph), −1.1 (6H, Ad), −7.1 (12H, Ph) (isopropyl methine resonance is not observed). UV−vis (C_6H_6) λ_{max}, nm (ε, L mol^{-1} cm^{-1}): 503 (1200), 670 (300). Evans' method (C_6D_6): 4.62 μ_B. Anal. Calcd for $C_{55}H_{66}FFe_2N_4P_3$: C, 65.62; H, 6.61; N, 5.57. Found: C, 65.67; H, 6.74; N, 5.38%.

F−Fe(^{i}PrNPPh$_2$)$_3$Fe(CO)$_2$ (**5**). Complex **3** (0.20 g, 0.22 mmol) was dissolved in benzene (10 mL) in a 50 mL Schlenk tube. The solution was frozen, and the headspace was evacuated and refilled with CO. The brown solution was warmed to room temperature and stirred under a CO atmosphere for 1 h to ensure the completion of the reaction, generating red complex **5**. The volatiles were removed in vacuo, and the crude material was washed with cold pentane. Extraction of the remaining red material into Et_2O, followed by removal of the solvent in vacuo, yielded analytically pure **5** (0.16 g, 80%). X-ray quality single crystals of **5** were grown from a concentrated Et_2O solution of **5** at −32 °C. ^1H NMR (400 MHz, C_6D_6): δ 16.0 (18H, ^{i}Pr−CH_3), 7.2 (6H, Ph), 4.8 (12H, Ph), 1.7 (12H, Ph) (isopropyl methine resonance is not observed). IR (KBr solution cell, benzene): 1982, 1921 cm^{-1}. UV−vis (C_6H_6) λ_{max}, nm (ε, L mol^{-1} cm^{-1}): 380 (9200), 493 (1200), 878 (150). Evans' method (C_6D_6): 4.86 μ_B. Anal. Calcd for $C_{47}H_{51}FFe_2N_3O_2P_3$: C, 61.79; H, 5.63; N, 4.60. Found: C, 61.69; H, 5.68; N, 4.53%.

F−Fe(^{i}PrNPPh$_2$)$_3$Fe(CN^{t}Bu)$_2$ (**6**). A solution of ^{t}BuNC (120 μL, 1.1 mmol) in benzene (3 mL) was chilled to −32 °C, and to this a benzene solution of **3** (0.33 g, 0.35 mmol) was added dropwise over the period of 5 min. The reaction mixture immediately turned red and was continuously stirred for 30 min to ensure completion of the reaction. Volatiles were removed in vacuo, and the crude materials were washed with pentane. Complex **6** was obtained as an analytically pure red crystalline material by slow evaporation of a concentrated Et_2O solution at room temperature (0.28 g, 78%). ^1H NMR (400 MHz, C_6D_6): δ 16.3 (18H, ^{i}Pr−CH_3), 7.2 (6H, Ph), 3.8 (12H, Ph), 1.7 (12H, Ph), 0.8 (18H, ^{t}Bu), (isopropyl methine resonance is not observed). IR (KBr solution cell, benzene): 1960, 1816 cm^{-1}. UV−vis (C_6H_6) λ_{max}, nm (ε, L mol^{-1} cm^{-1}): 367 (5300), 486 (1700), 672 (180). Evans method (C_6D_6): 4.89 μ_B. Anal. Calcd for $C_{55}H_{69}FFe_2N_5P_3$: C, 64.52; H, 6.79; N, 6.84. Found: C, 64.44; H, 6.72; N, 6.77%.

■ ASSOCIATED CONTENT

Supporting Information

Additional spectroscopic data, computational details, and crystallographic data in CIF format. This material is available free of charge via the Internet at http://pubs.acs.org.

■ AUTHOR INFORMATION

Corresponding Author

*E-mail: thomasc@brandeis.edu.

Notes

The authors declare no competing financial interest.

■ ACKNOWLEDGMENTS

This material is based upon work supported by Brandeis University and, under Award No. DE-SC0004019, the Department of Energy. C.M.T. and L.A.B. are Alfred P. Sloan Foundation Fellows. The authors also thank Dr. T. A. Betley (Harvard University) for assistance with Mössbauer spectroscopy and Dr. M. Dincă (MIT) for access to computational resources for Mössbauer calculations. J.M.K would like to thank Colgate University for startup funding.

■ REFERENCES

(1) Saouma, C. T.; Peters, J. C. *Coord. Chem. Rev.* **2011**, *255*, 920−937.
(2) Mehn, M. P.; Peters, J. C. *J. Inorg. Biochem.* **2006**, *100*, 634−643.
(3) Eikey, R. A.; Abu-Omar, M. M. *Coord. Chem. Rev.* **2003**, *243*, 83−124.
(4) Jung, N.; Bräse, S. *Angew. Chem., Int. Ed.* **2012**, *51*, 5538−5540.
(5) Ray, K.; Heims, F.; Pfaff, F. F. *Eur. J. Inorg. Chem.* **2013**, *2013*, 3784−3807.
(6) Berry, J. F. *Comments Inorg. Chem.* **2009**, *30*, 28−66.
(7) Zhang, L.; Deng, L. *Chin. Sci. Bull.* **2012**, *57*, 2352−2360.
(8) Che, C.-M.; Zhou, C.-Y.; Wong, E.-M. *Iron Catalysis;* Plietker, B., Ed.; Springer: Berlin, Heidelberg, 2011; Vol. *33*, p 111−138.
(9) Hohenberger, J.; Ray, K.; Meyer, K. *Nat. Commun.* **2012**, *3*, DOI: 10.1038/nscomms1718.
(10) Thomas, C. M.; Mankad, N. P.; Peters, J. C. *J. Am. Chem. Soc.* **2006**, *128*, 4956−4957.
(11) Brown, S. D.; Peters, J. C. *J. Am. Chem. Soc.* **2005**, *127*, 1913−1923.
(12) Nieto, I.; Ding, F.; Bontchev, R. P.; Wang, H.; Smith, J. M. *J. Am. Chem. Soc.* **2008**, *130*, 2716−2717.
(13) Brown, S. D.; Betley, T. A.; Peters, J. C. *J. Am. Chem. Soc.* **2003**, *125*, 322−323.
(14) Betley, T. A.; Peters, J. C. *J. Am. Chem. Soc.* **2003**, *125*, 10782−10783.
(15) Moret, M.-E.; Peters, J. C. *Angew. Chem., Int. Ed.* **2011**, *50*, 2063−2067.
(16) Bart, S. C.; Lobkovsky, E.; Bill, E.; Chirik, P. J. *J. Am. Chem. Soc.* **2006**, *128*, 5302−5303.
(17) Scepaniak, J. J.; Young, J. A.; Bontchev, R. P.; Smith, J. M. *Angew. Chem., Int. Ed.* **2009**, *48*, 3158−3160.
(18) Cowley, R. E.; DeYonker, N. J.; Eckert, N. A.; Cundari, T. R.; DeBeer, S.; Bill, E.; Ottenwaelder, X.; Flaschenriem, C.; Holland, P. L. *Inorg. Chem.* **2010**, *49*, 6172−6187.
(19) Bowman, A. C.; Milsmann, C.; Bill, E.; Turner, Z. R.; Lobkovsky, E.; DeBeer, S.; Wieghardt, K.; Chirik, P. J. *J. Am. Chem. Soc.* **2011**, *133*, 17353−17369.
(20) Lu, C. C.; Saouma, C. T.; Day, M. W.; Peters, J. C. *J. Am. Chem. Soc.* **2006**, *129*, 4−5.
(21) King, E. R.; Hennessy, E. T.; Betley, T. A. *J. Am. Chem. Soc.* **2011**, *133*, 4917−4923.
(22) Ni, C.; Fettinger, J. C.; Long, G. J.; Brynda, M.; Power, P. P. *Chem. Commun.* **2008**, 6045−6047.
(23) Verma, A. K.; Nazif, T. N.; Achim, C.; Lee, S. C. *J. Am. Chem. Soc.* **2000**, *122*, 11013−11014.
(24) Kuppuswamy, S.; Powers, T. M.; Johnson, B. M.; Bezpalko, M. W.; Brozek, C. K.; Foxman, B. M.; Berben, L. A.; Thomas, C. M. *Inorg. Chem.* **2013**, *52*, 4802−4811.
(25) Long, A. K. M.; Timmer, G. H.; Pap, J. S.; Snyder, J. L.; Yu, R. P.; Berry, J. F. *J. Am. Chem. Soc.* **2011**, *133*, 13138−13150.

(26) Pap, J. S.; DeBeer George, S.; Berry, J. F. *Angew. Chem., Int. Ed.* **2008**, *47*, 10102−10105.
(27) Nippe, M.; Goodman, S. M.; Fry, C. G.; Berry, J. F. *J. Am. Chem. Soc.* **2011**, *133*, 2856−2859.
(28) Berry, J. F. *Dalton Trans.* **2012**, *41*, 700−713.
(29) Cowley, R. E.; Eckert, N. A.; Elhaik, J.; Holland, P. L. *Chem. Commun.* **2009**, 1760−1762.
(30) Zhang, Q.; Xiang, L.; Deng, L. *Organometallics* **2012**, *31*, 4537−4543.
(31) Wertheim, G. K.; Herber, R. H. *J. Chem. Phys.* **1963**, *38*, 2106−2111.
(32) Scepaniak, J. J.; Harris, T. D.; Vogel, C. S.; Sutter, J.; Meyer, K.; Smith, J. M. *J. Am. Chem. Soc.* **2011**, *133*, 3824−3827.
(33) Scepaniak, J. J.; Vogel, C. S.; Khusniyarov, M. M.; Heinemann, F. W.; Meyer, K.; Smith, J. M. *Science* **2011**, *331*, 1049−1052.
(34) Hendrich, M. P.; Gunderson, W.; Behan, R. K.; Green, M. T.; Mehn, M. P.; Betley, T. A.; Lu, C. C.; Peters, J. C. *Proc. Natl. Acad. Sci. U. S. A.* **2006**, *103*, 17107−17112.
(35) Vogel, C.; Heinemann, F. W.; Sutter, J.; Anthon, C.; Meyer, K. *Angew. Chem., Int. Ed.* **2008**, *47*, 2681−2684.
(36) Kuppuswamy, S.; Bezpalko, M. W.; Powers, T. M.; Turnbull, M. M.; Foxman, B. M.; Thomas, C. M. *Inorg. Chem.* **2012**, *51*, 8225−8240.
(37) Kuppuswamy, S.; Cooper, B. G.; Bezpalko, M. W.; Foxman, B. M.; Powers, T. M.; Thomas, C. M. *Inorg. Chem.* **2012**, *51*, 1866−1873.
(38) Addison, A. W.; Rao, T. N.; Reedijk, J.; van Rijn, J.; Verschoor, G. C. *J. Chem. Soc., Dalton Trans.* **1984**, 1349−1356.
(39) Mock, M. T.; Popescu, C. V.; Yap, G. P. A.; Dougherty, W. G.; Riordan, C. G. *Inorg. Chem.* **2008**, *47*, 1889−1891.
(40) Tondreau, A. M.; Milsmann, C.; Lobkovsky, E.; Chirik, P. J. *Inorg. Chem.* **2011**, *50*, 9888−9895.
(41) Evans, D. F. *J. Chem. Soc.* **1959**, 2003−2005.
(42) Sur, S. K. *J. Magn. Reson.* **1989**, *82*, 169−173.
(43) *Apex 2: Version 2 User Manual, M86-E01078;* Bruker Analytical X-ray Systems: Madison, WI, 2006.
(44) Frisch, M. J.; Trucks, G. W.; Schlegel, H. B.; Scuseria, G. E.; Robb, M. A.; Cheeseman, J. R.; Scalmani, G.; Braone, V.; Mennucci, B.; Petersson, G. A., et al. *Gaussian 09, Revision A. 2;* Gaussian, Inc.: Wallingford, CT, 2009.
(45) Becke, A. D. *Phys. Rev. A: At., Mol., Opt. Phys.* **1988**, *38*, 3098−3100.
(46) Perdew, J. P. *Phys. Rev. B: Condens. Matter Mater. Phys.* **1986**, *33*, 8822−8824.
(47) Hay, P. J.; Wadt, W. R. *J. Chem. Phys.* **1985**, *82*, 299−310.
(48) Roy, L. E.; Hay, P. J.; Martin, R. L. *J. Chem. Theory Comput.* **2008**, *4*, 1029−1031.
(49) Ehlers, A. W.; Bohme, M.; Dapprich, S.; Gobbi, A.; Hollwarth, A.; Jonas, V.; Kohler, K. F.; Stegmann, R.; Veldkamp, A.; Frenking, G. *Chem. Phys. Lett.* **1993**, *208*, 111−114.
(50) Dunning, T. H., Jr.; Hay, P. J. In *Modern Theoretical Chemistry;* Schaefer, H. F., Ed.; Plenum: New York, 1976; Vol. 3.
(51) Neese, F. *ORCA—an ab initio, Density Funcional and Semieimpirical program package,* Version 2.9.1; Max Planck Institute for Bioinorganic Chemistry: Mulheim, Germany, 2012.
(52) Schäfer, A.; Horn, H.; Ahlrichs, R. *J. Chem. Phys.* **1992**, *97*, 2571−2577.